Solar-Driven Reversible Hydrogen Storage

Xiaoyue Zhang, Yahui Sun, Shunlong Ju, Jikai Ye, Xuechun Hu, Wei Chen, Long Yao, Guanglin Xia,* Fang Fang,* Dalin Sun, and Xuebin Yu*

The lack of safe and efficient hydrogen storage is a major bottleneck for large-scale application of hydrogen energy. Reversible hydrogen storage of light-weight metal hydrides with high theoretical gravimetric and volumetric hydrogen density is one ideal solution but requires extremely high operating temperature with large energy input. Herein, taking MgH_2 as an example, a concept is demonstrated to achieve solar-driven reversible hydrogen storage of metal hydrides via coupling the photothermal effect and catalytic role of Cu nanoparticles uniformly distributed on the surface of MXene nanosheets (Cu@MXene). The photothermal effect of Cu@MXene, coupled with the "heat isolator" role of MgH_2 indued by its poor thermal conductivity, effectively elevates the temperature of MgH_2 upon solar irradiation. The "hydrogen pump" effect of Ti and TiH_x species that are in situ formed on the surface of MXene from the reduction of MgH_2, on the other hand, plays a catalytic role in effectively alleviating the kinetic barrier and hence decreasing the operating temperature required for reversible hydrogen adsorption and desorption of MgH_2. Based on the combination of photothermal and catalytic effect of Cu@MXene, a reversible hydrogen storage capacity of 5.9 wt% is achieved for MgH_2 after 30 cycles using solar irradiation as the only energy source.

1. Introduction

The increasing global warming and energy crisis resulting from the use of conventional fossil fuels has motivated extensive exploration of renewable and sustainable clean energy.[1] Hydrogen has been widely regarded as a predominant candidate as a future energy carrier for sustainable development.[2] The lack of an effective and safe strategy to storage hydrogen with high gravimetric and volumetric density, however, poses a critical challenge for large-scale application of hydrogen energy.[3] Recently, storing hydrogen in solid-state light-weight metal hydrides has attracted increasing attention since it has unique safety characteristics endowed with ultrahigh theoretical gravimetric and volumetric hydrogen densities.[4] Nonetheless,

the reversible hydrogen uptake and release reaction of these metal hydrides is extremely endothermic in general with high kinetic barrier.[5] As a result, high operating temperature that is achieved by external heating using artificial energy (e.g., electricity in general), which would require large extra energy input and high operating costs for their large-scale application, is now a prerequisite for realizing reversible hydrogen storage of these metal hydrides. It would inevitably lower the hydrogen storage density and energy efficiency of the whole hydrogen storage system and more importantly, cannot eliminate our reliance on fossil fuels. Unfortunately, this major issue has been ignored for a long time. An alternative catalytic strategy that allows the reversible hydrogen storage of metal hydrides to be performed under mild reaction conditions with minimum energy and cost input is required in urgent.

Harnessing solar energy for energy storage has been widely regarded as a crucial pathway to alleviate the global energy shortage and environment pollution.[6] Therefore, the efficient utilization of renewable solar energy for reversible hydrogen storage is considered to be one of the most promising strategies to simultaneously mitigate the global energy crisis and increase the energy efficiency of hydrogen storage process. Recent progress of photothermal effect of metal-based catalysts based on electron oscillations under light excitation[7] and the localized surface plasmon resonance (LSPR) effect[8] demonstrates the generation of localized heating using the solar energy, which could be applied for initiating and driving reversible hydrogen storage of metal hydrides. Unfortunately, the research integrating photothermal features to realize photothermally assisted reversible hydrogen storage of metal hydrides has yet to be explored up to now as far as we know. The challenge regarding the capability of photothermal effect in realizing reversible hydrogen storage of metal hydrides remains to be resolved urgently.

Herein, taking advantage of MgH_2 as a model example, we demonstrate a concept to realize solar-driven reversible hydrogen storage of metal hydrides via coupling photothermal and catalytic effect of Cu nanoparticles uniformly supported on MXene (Cu@MXene). First, outstanding photothermal conversion capabilities of Cu@MXene based on the combination of the plasmonic properties of Cu nanoparticles and the

X. Zhang, Y. Sun, S. Ju, J. Ye, X. Hu, W. Chen, L. Yao, G. Xia, F. Fang, D. Sun, X. Yu
Department of Materials Science
Fudan University
Shanghai 200433, China
E-mail: xiaguanglin@fudan.edu.cn; f_fang@fudan.edu.cn; yuxuebin@fudan.edu.cn

**ADVANCED
SCIENCE NEWS**

www.advancedsciencenews.com

**ADVANCED
MATERIALS**

www.advmat.de

photothermal effect and high thermal conductivity of MXene nanosheets are adopted to generate localized heat under solar irradiation for driving H_2 desorption and adsorption of MgH_2. On the other hand, the "hydrogen pump" effect of Ti and TiH_x species that are in situ formed on the surface of MXene from the reduction of MgH_2 is capable of effectively weakening Mg−H bonds and mitigating relative energy barrier of H_2 desorption from MgH_2, which hence plays a catalytic role in effectively decreasing the operating temperature required for dehydrogenation and hydrogenation of MgH_2. Coincidently, MgH_2 has a poor thermal conductivity and hence it could act as "heat isolator" to reduce the temperature gradient near Cu@MXene that serves as the photothermal and catalytic sites, which contributes to driving fast H_2 desorption and absorption of MgH_2. As a result, in comparison to the typical thermal-promoted solid-state hydrogen storage reaction, the combination of photothermal conversion with catalytic effect allows Cu@MXene to collect a heating source to reduce the temperature gradient near catalytic center and get a higher reactivity at local sites, resulting in faster response of H_2 desorption to the solar irradiation than that of traditional thermal heating. Accordingly, using solar energy only, stable reversible hydrogen desorption and adsorption could be facile achieved for MgH_2 under the catalysis of Cu@MXene, delivering a high H_2 storage capacity of 5.9 wt% after 30 cycles.

2. Results and Discussion

2.1. Preparation and Characterization of Cu@MXene

The fabrication process of Cu@MXene is schematically illustrated in **Figure 1**a, in which the few-layer MXene ($Ti_3C_2T_x$) dispersed in deionized water is first prepared by etching the MAX phase and ultrasonication. After the etching process of MAX phase, X-ray diffraction (XRD) pattern illustrates the (002) characteristic peak of MXene located at 8.14° (Figure 1b), indicating the formation of MXene. Subsequently, the positively charged Cu^{2+} is introduced to uniformly coordinate with the negatively charged −OH functional group of MXene to realize electrostatic self-assembly of Cu^{2+} ions, which results in the homogeneous anchoring of Cu nanoparticles on the surface of MXene sheets after thermal annealing. As evidenced by the XRD results, three peaks located at 43.19°, 50.20°, and 73.89°could be indexed to the (111), (200), and (220) planes of the fcc-structured Cu, respectively, indicating the presence of Cu nanoparticles inside of Cu@MXene. In addition, the (002) characteristic peak of MXene is shifted from 8.14° for MXene to 8.08° for Cu@MXene, indicating the enlargement of the *d*-spacing of MXene nanosheets[9] due to the uniform anchoring of Cu nanoparticles on the surface of MXene nanosheets, which would increase the interlayer spacing to prevent the restacking of MXene sheets in Cu@MXene.[10] Moreover, X-ray photoelectron spectroscopy (XPS) measurement of MXene and Cu@MXene illustrates characteristic peaks of C 1s, O 1s, Ti 2p, Ti 3p, and F 1s (Figure 1c; Figure S1, Supporting Information). In comparison to pure MXene, an extra energy band at around 929.3 eV associated with the characteristic peak of Cu 2p could be observed for Cu@MXene.[11] Two characteristic peaks located at 931.2 eV and

951.1 eV in Cu 2p XPS spectrum of Cu@MXene (Figure 1d), corresponding to the binding energies of Cu^0 $2p_{3/2}$ and Cu^0 $2p_{1/2}$, respectively, provide additional evidence to the presence of zero-valent copper.[12]

Scanning electron microscopy (SEM) images of Cu@MXene (Figure 1e) illustrate that the layered structures of MXene are well preserved with the homogeneous anchoring of Cu nanoparticles, possessing particle sizes ranging from 10 to 20 nm. High-resolution transmission electron microscopy (HRTEM) (Figure 1f) image of these Cu nanoparticles exhibits the lattice fringes of approximately 0.21 nm, corresponding to the (111) plane of Cu, which directly confirms the uniform formation of Cu nanoparticles on the surface of MXene sheets. The interlayer spacing of MXene is calculated to be 1.12 nm (Figure S2, Supporting Information), which is in good agreement with the (002) peak of MXene as verified by the XRD results (Figure 1b). In addition, the energy dispersive X-ray spectroscopy (EDS) elemental mapping (Figure 1g) confirms the homogeneous distribution of Ti, C, and Cu, further validating the uniform dispersion of Cu nanoparticles on the surface of MXene nanosheets. The loading ratio of Cu nanoparticles is determined to be 7 wt% by inductively coupled plasma source mass spectrometer (ICP-MS) with the detection of a small amount element of O (10.61%), Cl (1.70%), F (1.50%), and N (1.07%) (Figure S3 and Table S1, Supporting Information), which could be attributed to the natural functional groups on MXene surface.[13] These results demonstrate the homogeneous synthesis of Cu nanoparticles on the surface of MXene nanosheets.

2.2. Photothermal Effect of Cu@MXene

UV–vis–NIR absorption spectra of Cu@MXene and MXene (**Figure 2**a) illustrate that Cu@MXene exhibits an overall stronger absorption than that of pure MXene in the visible and near-infrared wavelength ranges.[14] Two absorption peaks between 400 and 1200 nm owing to the strong enhancement of light–matter interaction by the LSPR effect could be clearly observed for pure MXene, which hence could serve as the light absorber.[15] Due to this LSPR-like photothermal effect[16] and nearly 100% internal light-to-heat conversion efficiency,[17] the temperature of MXene reaches 246.0 °C under a light intensity of 1.39 W cm^{-2} (Figure 2b; Figure S4, Supporting Information). It is noteworthy that the characteristic absorption peak of MXene in the visible range has a red shift from 550 to 590 nm after the homogeneous decoration of Cu nanoparticles,[18] which could be induced by the absorption contribution of the LSPR effect of Cu nanoparticles located at ~590 nm.[19] As a result, the temperature could be elevated to 263.7 °C for Cu@MXene under the identical condition with that of MXene, which directly validates the stronger LSPR response effect of Cu@MXene due to the combination of the plasmonic properties of Cu nanoparticles and the photothermal effect of MXene nanosheets as the photothermal carrier.[20] Moreover, the temperature of Cu@MXene is always higher than that of MXene under various irradiation intensities between 1.39 and 1.92 W cm^{-2}, exhibiting a linear relationship between the surface temperature and irradiation intensity for both Cu@MXene and MXene.[21] The larger slope of Cu@MXene than
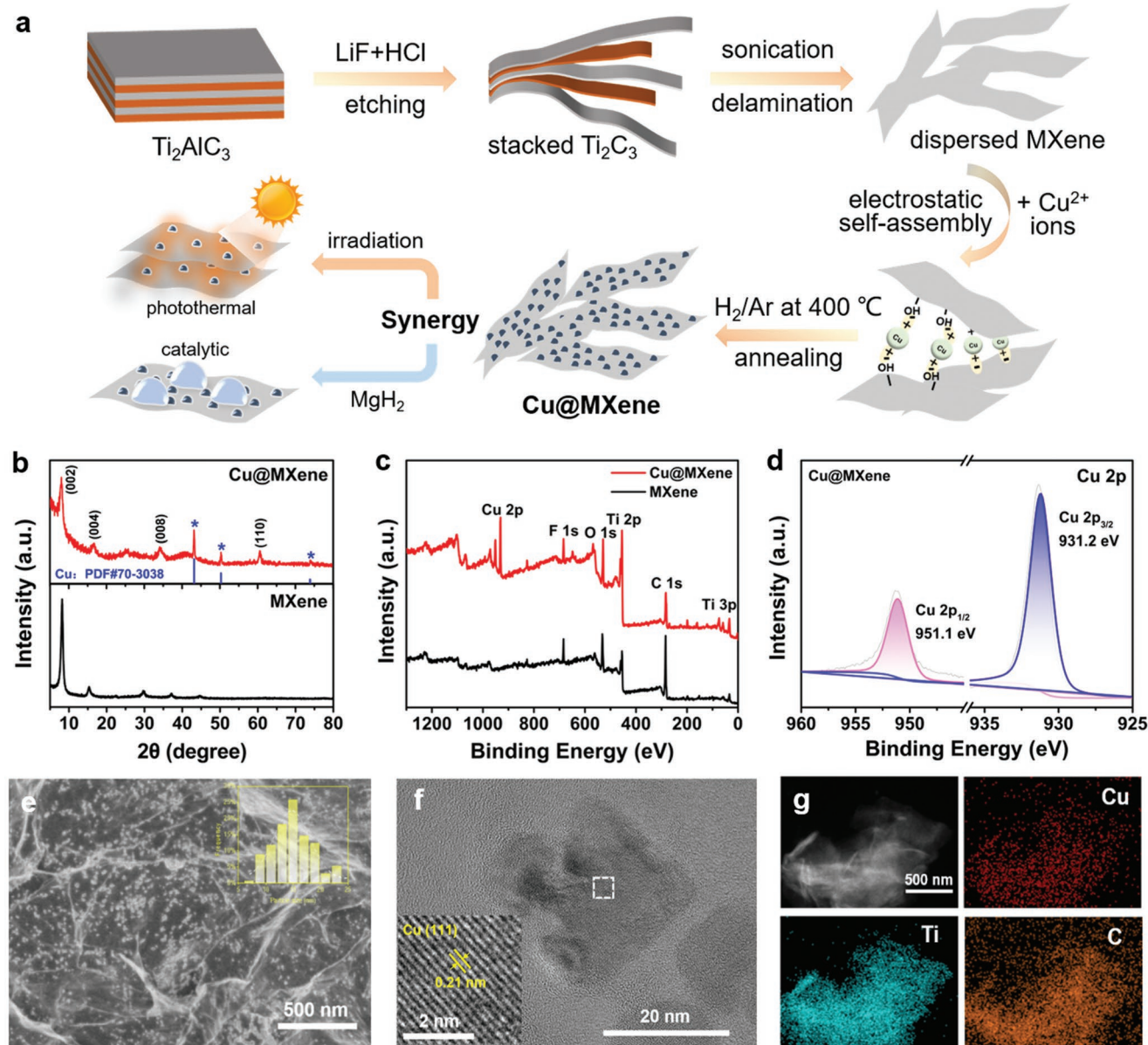
Figure 1. a) Schematic illustration of the fabrication of Cu@MXene. b) XRD patterns and c) XPS survey spectra of the as-synthesized Cu@MXene and MXene. d) High-resolution Cu 2p XPS spectrum of Cu@MXene. e) SEM image of Cu@MXene. The inset histogram shows the corresponding particle size distribution of Cu nanoparticles of Cu@MXene. f) TEM image of Cu nanoparticles in Cu@MXene. g) EDS elemental mapping images of Cu@MXene.

pure MXene within the test range demonstrates that more heat could be generated for Cu@MXene with the increase of irradiation intensity under identical condition, which provides additional evidence to the stronger photothermal conversion ability of Cu@MXene.[22] Particularly, an ultrahigh temperature of 330.4 °C could be achieved for Cu@MXene under an irradiation intensity of 1.92 W cm^{-2}. Moreover, a relatively stable temperature could be obtained for Cu@MXene within ~50 s (Figure S5a, Supporting Information), and this phenomenon is well preserved upon continuously adjusting the light intensity (Figure S5b, Supporting Information), indicating the fast response of the surface temperature of Cu@MXene to solar

irradiation. In addition, light-triggered cycling tests were performed on Cu@MXene under a light intensity of 1.60 W cm^{-2}, in which each cycle is composed of irradiating for about 90 s and cooling to below 53 °C for 60 s. As shown in Figure S6, Supporting Information, no deterioration on the temperature of Cu@MXene could be detected after ten cycles of irradiation and cooling process, indicating its superior fatigue-free photothermal performance.

In order to visually validate the superior photothermal effect of Cu@MXene than that of MXene, the temperature of Cu@MXene and MXene over the time were in situ captured via an infrared camera under a 0.40 W cm^{-2} full-spectrum light

**ADVANCED
SCIENCE NEWS**

www.advancedsciencenews.com
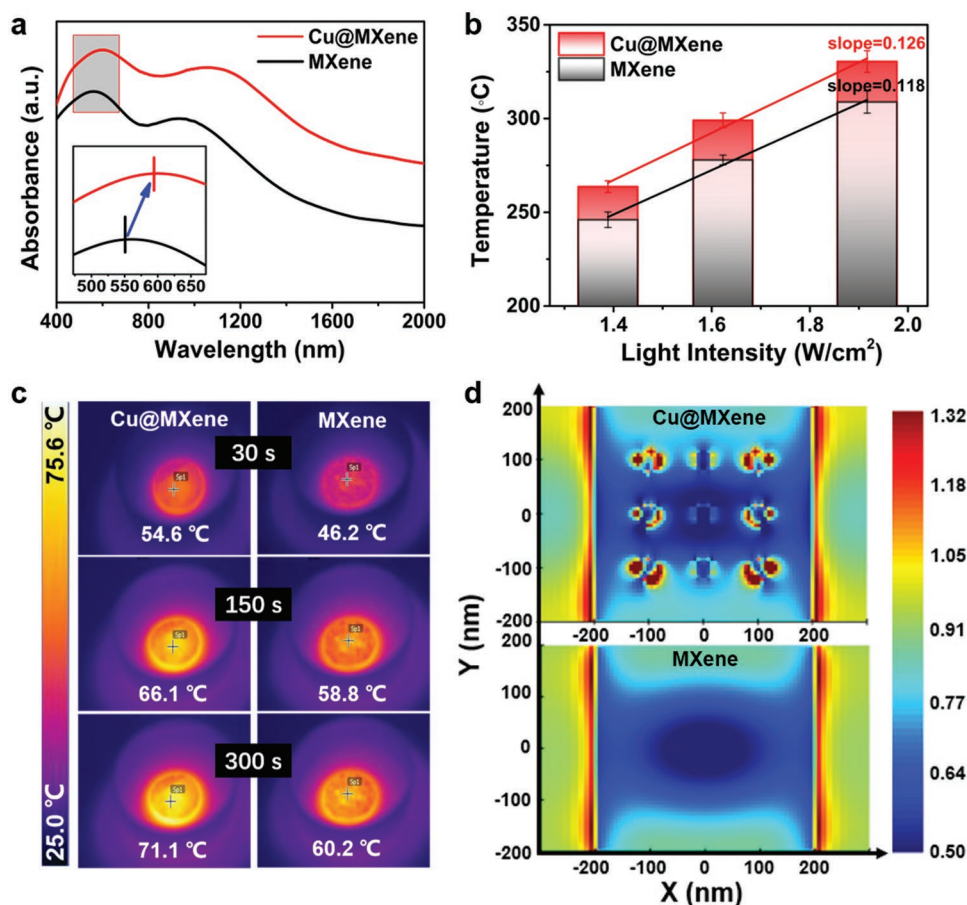
**ADVANCED
MATERIALS**

www.advmat.de

Figure 2. a) UV–vis–NIR absorption spectra of Cu@MXene and MXene. b) The relationship between the temperature and the light intensity observed for Cu@MXene and MXene after an irradiation time of 120 s. c) In situ detection of surface temperature of Cu@MXene and MXene recorded by an infrared thermal imager under a light intensity of 0.4 W cm^{-2}. d) FDTD simulated localized electric field enhancement profiles.

(Videos S1 and S2, Supporting Information). During 5 min of irradiation, the maximum surface temperature of Cu@MXene is always higher than that of pure MXene, with a more uniform thermal field distribution observed inside of Cu@MXene (Figure 2c). This phenomenon confirms the enhanced light-to-heat conversion of MXene due to the uniform decoration of Cu nanoparticles. To understand the mechanism behind the enhanced photothermal effect of Cu@MXene, finite-difference-time-domain (FDTD) simulations were performed to investigate the radiation energy transformation of Cu@MXene and MXene (Figure 2d; Figure S7, Supporting Information). In comparison to pure MXene nanosheets, plasmonic "hot spot" regions could be clearly observed near each Cu nanoparticle, which directly validates that the strong LSPR-induced localized electric-field of Cu nanoparticles results in higher temperature than that of MXene nanosheets. In addition, due to the high thermal conductivity of MXene nanosheets (Table S2, Supporting Information), the heat generated by the strong LSPR effect of Cu nanoparticles could be facilely diffused into MXene nanosheets, which contributes to uniformly enhancing the photothermal effect of MXene due to the homogeneous distribution of Cu nanoparticles on their surface. Induced by the synergistic LSPR coupling effect between Cu nanoparticles and MXene nanosheets, Cu@MXene exhibits stronger light absorption ability in the full spectral range than pure MXene nanosheets.

2.3. Catalytic Effect of Cu@MXene

Magnesium hydride (MgH$_2$), as one of the most promising solid-state light-weight metal hydrides, has advantages of high hydrogen capacity, excellent reversibility, and low cost,[23] but facing the serious challenges of the high operating temperature and slow kinetics due to its high thermodynamic stability ($\Delta H = 76$ kJ mol^{-1}) and kinetic barrier ($E_a = 160$ kJ mol^{-1}).[24] Introducing metal-based catalysts has been demonstrated as one of the most effective strategies to alleviate the kinetic barrier for reversible hydrogen storage of MgH$_2$, which could effectively decrease its operating temperature for H$_2$ desorption and adsorption.[25] Therefore, the effect of Cu@MXene in improving hydrogen storage performance of MgH$_2$ is first evaluated by means of traditional electric heating, in which the amount of introduced catalysts is controlled to be 10 wt%. Temperature-programmed desorption (TPD) results and their differential curves (Figure S8, Supporting Information) illustrate that the onset and peak dehydrogenation temperatures of ball-milled MgH$_2$ reach 315 and 347 °C, respectively, and hence a

large energy input would be required to drive H_2 desorption of MgH_2. In strong contrast, the introduction of both Cu@MXene and MXene results in a significant decrease of both onset and peak temperature for H_2 desorption from MgH_2. Particularly, the peak temperature for H_2 desorption from MgH_2 could be decreased to 237 and 248 °C under the catalysis of Cu@MXene and MXene, respectively, and both of them are ~100 °C lower than that of ball-milled MgH_2. It should be noted that the peak temperature for H_2 desorption from MgH_2 under the catalysis of Cu nanoparticles is comparable to pure MgH_2 (Figure S8a, Supporting Information), indicating that Cu nanoparticles is inactive in enhancing H_2 desorption performance of MgH_2. Hence, it indirectly demonstrates the catalytic role of Cu@MXene and MXene in effectively improving the H_2 storage performance of MgH_2 could be attributed to the presence of MXene.

To quantitatively evaluate the enhanced H_2 desorption performance of MgH_2 induced by the introduction of Cu@MXene, the activation energy (E_a) for dehydrogenation of MgH_2 is calculated using the Kissinger equation (Equation (S4), Supporting Information). According to the Kissinger's plots based on various heating rates (Figures S8c and S9, Supporting Information), the activation energies (E_a) for H_2 desorption from MgH_2 with the addition of MXene and Cu@MXene are determined to be 86.62 ± 2.26 and 90.46 ± 3.26 kJ mol^{-1}, respectively, both of which are significantly lower than that of ball-milled MgH_2 (136.69 ± 6.46 kJ mol^{-1}). The activation energy for H_2 desorption of MgH_2 under the catalysis of Cu@MXene, however, is slightly higher than that of MXene, which could be attributed to the partial replacement of MXene by Cu nanoparticles that have no catalytic effect in enhancing H_2 desorption performance of MgH_2 (Figure S8b, Supporting Information).

Isothermal H_2 desorption kinetics of MgH_2 catalyzed by Cu@MXene is subsequently evaluated at various temperatures. Upon heating at 240 °C (**Figure 3**a), H_2 desorption capacity released from MgH_2 under the catalysis of Cu@MXene and MXene reaches 6.3 and 5.5 wt% within the period of only 10 min, while almost no hydrogen could be released from
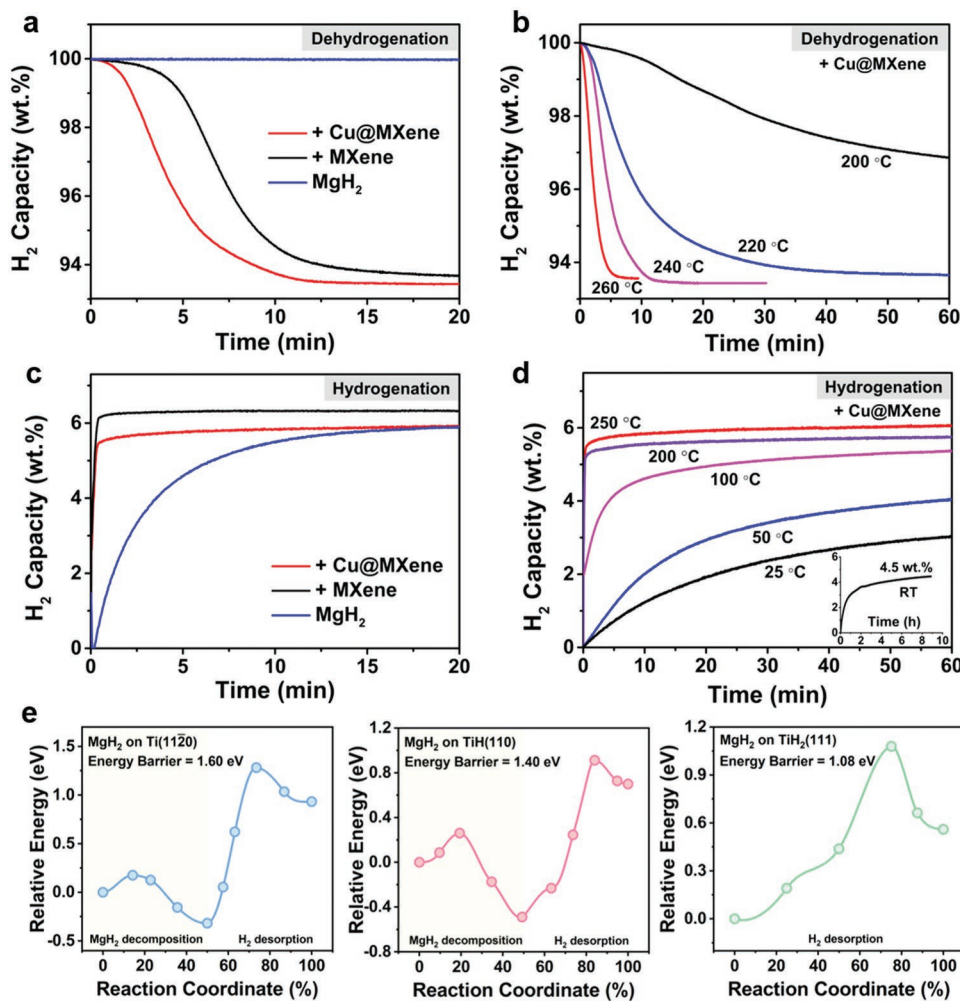

Figure 3. a) Isothermal dehydrogenation curves at 240 °C of MgH_2 under the catalysis of Cu@MXene and MXene, respectively, including ball-milled MgH_2 for comparison. b) Isothermal dehydrogenation profiles of MgH_2 under the catalysis of Cu@MXene at various temperatures. c) Isothermal hydrogenation curves at 250 °C of MgH_2 under the catalysis of Cu@MXene and MXene, respectively, including ball-milled MgH_2 for comparison. d) Isothermal hydrogenation curves of MgH_2 under the catalysis of Cu@MXene at various temperatures. e) Calculated energy profiles for the release of one H_2 molecule from MgH_2 under the catalysis of Ti, TiH, and TiH_2, respectively.

**ADVANCED
SCIENCE NEWS**

www.advancedsciencenews.com

**ADVANCED
MATERIALS**

www.advmat.de

ball-milled MgH$_2$ under the identical condition. This confirms the catalytic role of Cu@MXene and MXene in enhancing H$_2$ desorption performance of MgH$_2$. As expected, the increase of operating temperature leads to the enhanced H$_2$ desorption kinetics of MgH$_2$ catalyzed by Cu@MXene (Figure 3b). Particularly, a capacity of ~6.5 wt%, approaching the theoretical value of MgH$_2$ catalyzed by Cu@MXene, could be released within 300 s only at 260 °C. The apparent E_a of MgH$_2$ under the catalysis of Cu@MXene estimated by the Johnson–Mehl–Avrami (JMA) equation and the Arrhenius equation (Figure S10, Supporting Information) is calculated to be 90.31 ± 5.36 kJ mol^{-1}, consistent with that calculated by the Kissinger equation, which is among the best reported Ti-based catalyst for MgH$_2$ hydrogen storage materials so far (Table S3, Supporting Information). During the reversible H$_2$ adsorption process at 250 °C under 3 MPa H$_2$, only a capacity of 5.9 wt% H$_2$, corresponding to only 79% of its theoretical maximum capacity, could be adsorbed by pristine Mg within 60 min (Figure 3c). By comparison, the H$_2$ adsorption capacity of Mg under the catalysis of MXene and Cu@MXene reaches 6.0 wt% (about 93% of its maximum capacity) and 5.6 wt%, respectively, under the identical condition within 60 s only. Impressively, 5.0 wt% H$_2$ could be reversibly stored into Mg under the catalysis of Cu@MXene within 60 min upon decreasing the operating temperature down to 100 °C and, even at room temperature, it could adsorb 4.5 wt% of H$_2$ upon extending the reaction time to 8 h (Figure 3d). These results validate the effective catalytic role of Cu@MXene in simultaneously improving the H$_2$ desorption and adsorption kinetics of MgH$_2$.

Isothermal cycling H$_2$ absorption and desorption measurements illustrate that a reversible H$_2$ storage capacity of 6.1 wt% could be preserved for MgH$_2$ under the catalysis of Cu@MXene after 10 cycles (Figure S11, Supporting Information), corresponding to a high capacity retention of 93%. Only characteristic peaks of MgH$_2$ could be detected for MgH$_2$ catalyzed Cu@MXene after 10 cycles of hydrogenation process, with the reversible formation of Mg after cycling H$_2$ desorption, which confirms the excellent cycling stability of MgH$_2$ under the catalysis of Cu@MXene (Figure S12, Supporting Information). The characteristic peaks of MXene and Cu, however, could not be observed under the strong diffraction signals of Mg and MgH$_2$, which could be attributed to their amorphous state and/or low contents.[26] Fortunately, Ti 1p and C 1s XPS results of MgH$_2$ under the catalysis of Cu@MXene confirm the presence of Ti−C bonds of MXene and zero-valence Cu of Cu nanoparticles before and after cycling H$_2$ desorption and adsorption process, indicating the maintenance of Cu nanoparticles and partial MXene after cycling. In addition, upon the cycling H$_2$ adsorption and desorption process, the characteristic peak of Ti−C bonds of MXene remains almost unchanged, which provides additional evidence to the well-preservation of partial MXene during cycling hydrogen storage process. The continuous presence of MXene could exert their photothermal functions upon light irradiation during reversible hydrogen storage process (Figures S13, Supporting Information). In addition, only weak peaks of Ti−O bonds, accompanied with the presence of MgO, could be observed in the O 1s XPS spectra of MgH$_2$ under the catalysis of Cu@MXene, which could be attributed to the partial reaction between MgH$_2$ and MXene and/or the inevitable oxidation during the sample transfer process. In addition, the characteristic peaks of metallic Ti^0 at 459.4 and 453.4 eV could also be observed for MgH$_2$ under the catalysis of Cu@MXene after the ball-milling process, indicating the in situ formation of metallic Ti, which could be attributed to partial reduction of MXene by MgH$_2$.[27] Interestingly, the hydrogenation process leads to the formation of Ti−H bonds observed at 459.9 and 453.9 eV with the almost disappearance of metallic Ti, indicating the presence of "hydrogen pump" effect based on the transformation between Ti and TiH$_x$ during reversible hydrogen storage process of MgH$_2$, which holds great potential to improve the H$_2$ release and uptake performance of MgH$_2$. It could be supported by the significant decrease of the peak temperature for the dehydrogenation of MgH$_2$ down to 316 °C after the addition of commercial Ti nanoparticles (Figure S8a, Supporting Information), which directly demonstrates the catalytic effect of Ti in improving H$_2$ desorption performance of MgH$_2$. The peak temperature for H$_2$ desorption from MgH$_2$ catalyzed by both Cu@MXene and MXene, however, is much lower than that of MgH$_2$ catalyzed by Ti nanoparticles, which confirms that the in situ formation of Ti from the reaction between MgH$_2$ and MXene could enhance the catalytic effect of Ti in improving H$_2$ desorption performance of MgH$_2$.

In order to unravel the catalytic role of Ti and TiH$_x$ based on their "hydrogen pump" effect, theoretical calculations were conducted based on density functional theory (DFT). It is revealed that the length of Mg−H bonds in the pristine MgH$_2$ monomer is 1.71 Å. Under the support of both Ti and TiH$_x$ species, the corresponding Mg−H bonds are stretched and an obvious increase of 0.21 Å could be observed for MgH$_2$ under the catalysis of TiH, indicating that both Ti and TiH$_x$ are capable of effectively weakening Mg−H bonds (Figure S14, Supporting Information). As evidenced by charge density difference analysis, it could be attributed to the charge transfer between Ti and TiH$_x$ species and MgH$_2$, where the charges accumulate in the interfacial spaces and deplete in the area between Mg and H atoms, indicating the decrease of ionic interaction of MgH$_2$ molecule. To quantitively understand the catalytic effect of Ti and TiH$_x$, the H$_2$ desorption barrier for MgH$_2$ is subsequently calculated. In the term of MgH$_2$, the relative energy barrier for H$_2$ desorption from MgH$_2$ reaches 3.12 eV (Figure S15a, Supporting Information), indicating the presence of large kinetic barrier for its hydrogen storage reaction, which correlates well with its high H$_2$ desorption temperature of over 370 °C (Figure S8, Supporting Information). Interestingly, the presence of Ti and TiH$_x$ species leads to the significant decrease of the H$_2$ desorption barrier of MgH$_2$. More importantly, in comparison to metallic Ti, the catalysis of TiH$_2$ and TiH, which are in situ formed during the formation of MgH$_2$ from the reversible H$_2$ adsorption process as verified by the XPS results (Figure S13, Supporting Information), is most effective in reducing the H$_2$ desorption barrier of MgH$_2$, which could be even decreased to 1.08 eV under the catalysis of TiH$_2$. The release of H$_2$ from MgH$_2$ hence could be effectively promoted at its initial state of dehydrogenation. Considering the much lower H$_2$ desorption barrier of TiH$_2$ (i.e., 1.35 eV) than that of MgH$_2$ (i.e., 3.12 eV) (Figure S15a, Supporting Information), the formation of Ti or TiH from self-dehydrogenation of TiH$_2$ is inevitable and hence the catalytic effect of Ti or TiH in enhancing the H$_2$ desorption

**ADVANCED
SCIENCE NEWS**

www.advancedsciencenews.com

**ADVANCED
MATERIALS**

www.advmat.de

performance of MgH$_2$ should be further evaluated. Impressively, under a stable structural configuration, the hydrogen of MgH$_2$ would be spontaneously transferred into Ti and/or TiH matrix, which directly demonstrates the "hydrogen pump" effect of Ti and TiH$_x$ species. Moreover, the release of this transferred hydrogen would be significantly reduced to 1.60 and 1.40 eV under the catalysis of Ti and TiH, respectively, much lower than that of pure MgH$_2$ (i.e., 3.12 eV), directly validating the important role of the "hydrogen pump" effect of Ti and TiH$_x$ species in promoting the H$_2$ desorption performance of MgH$_2$ (Figure 3e). Coincidentally, the in situ formation of Ti and TiH$_x$ species on the surface of MXene nanosheets from the reduction of MgH$_2$ could ensure their homogenous distribution inside of MgH$_2$ with intimate contact, which would effectively promote their catalytic effect in improving the H$_2$ storage performance of MgH$_2$.

2.4. Reversible Hydrogen Storage of MgH$_2$ Driven by Solar Energy

Based on the photothermal performance of Cu@MXene and the hydrogen storage performance of MgH$_2$ under the catalysis of Cu@MXene, it is concluded that the heat generated by Cu@MXene under solar irradiation, coupled with its catalytic effect in improving H$_2$ storage performance of MgH$_2$, is capable of driving the reversible H$_2$ storage of MgH$_2$. Hence, a customized solar-driven H$_2$ absorption and desorption equipment was built to investigate the solar-driven H$_2$ storage performance of MgH$_2$ (Figure S16, Supporting Information). Owing to the introduction of Cu@MXene with strong light adsorption ability (Figure S17, Supporting Information), the surface temperature of MgH$_2$ under the catalysis of Cu@MXene approaches 209 °C within 5 min under a light intensity of 2.61 W cm^{-2}, which is able to thermally drive H$_2$ desorption of MgH$_2$ catalyzed by Cu@MXene (**Figure 4**a). In response to this irradiation, rapid H$_2$ desorption with a capacity of 3.9 wt% H$_2$ could be clearly observed for MgH$_2$ under the catalysis of Cu@MXene (Figure 4b). By comparison, since MXene exhibits comparable catalytic effect in improving H$_2$ storage performance of MgH$_2$ with Cu@MXene but with relatively weaker light absorption ability, only a temperature of 200 °C could be achieved, resulting in the release of H$_2$ with a capacity of only 3.0 wt%, which is ~1.0 wt% less than that of MgH$_2$ catalyzed by Cu@MXene. More interestingly, under the light intensity of 2.61 W cm^{-2}, the surface temperature of MgH$_2$ with the addition of Cu nanoparticles reaches 243 °C (Figure S18a, Supporting Information), much higher than that of Cu@MXene (i.e., 209 °C). This result provides direct evidence to the strong LSPR effect of Cu nanoparticles, which could be further supported by the obvious absorption peak at around 600 nm in visible light range detected by UV–vis–NIR (Figure S18c, Supporting Information), in elevating the temperature of MgH$_2$. Hence, the temperature of Cu@MXene under the identical light irradiation is much higher than that of MXene due to the uniform decoration of Cu nanoparticles on the surface of MXene. In addition, induced by the LSPR effect of Ti nanoparticles, the surface temperature of MgH$_2$ with the addition of Ti nanoparticles is also comparable to that of Cu@MXene. Although the surface temperature of MgH$_2$ with the

addition of Ti nanoparticles or Cu nanoparticles is comparable to or even much higher than that of MgH$_2$ with the addition of Cu@MXene under the light intensity of 2.61 W cm^{-2}, the H$_2$ capacity released from MgH$_2$ catalyzed by Cu nanoparticles and Ti nanoparticles (Figure S18b, Supporting Information) is only 0.56 and 0.95 wt%, respectively, which could be attributed to their limited catalytic effect in improving H$_2$ desorption performance of MgH$_2$. These results confirm the synergistic effect of the photothermal and catalytic role of Cu@MXene is capable of achieving H$_2$ desorption of MgH$_2$ using solar irradiation only. Furthermore, with the increase of light intensity, the temperature of MgH$_2$ increases (Figure 4c), which would increase the degree of H$_2$ desorption from MgH$_2$ (Figure 4d; Figure S19, Supporting Information). Particularly, a complete dehydrogenation of MgH$_2$ with a capacity of 6.2 wt% could be achieved within 60 min under a light intensity of 3.10 W cm^{-2}, and a faster H$_2$ release kinetics with almost constant amount of hydrogen desorption is observed upon increasing the light intensity to 3.35 W cm^{-2}.

It could be noted that the dehydrogenation rate has an exponential relationship with the light intensity (Figure S20a, Supporting Information), indicating that the photothermal effect mainly accounts for the increase of dehydrogenation rate.[28] Comparing the amount of H$_2$ desorption at various temperatures (Figure S20b, Supporting Information), the H$_2$ desorption performance under solar energy is similar to that driven by thermal heating, that is, MgH$_2$ releases hydrogen through a photothermal pathway induced by the light-to-heat conversion ability of Cu@MXene rather than photocatalytic principle.[29] In addition, the apparent activation energy under light irradiation is calculated to be 86.49 ± 4.98 kJ mol^{-1}, which is comparable to that driven by thermal heating (i.e., 90.31 ± 5.36 kJ mol^{-1}) (Figure S20c, Supporting Information). These results validate that the solar-driven dehydrogenation of MgH$_2$ is mainly achieved based on heat produced by photothermal effect of Cu@MXene with the combination of its catalytic effect. In strong contrast, no hydrogen release could be observed for ball-milled MgH$_2$ even under a high light intensity of 3.35 W cm^{-2}, which provides direct evidence to the important role of Cu@MXene based on its photothermal and catalytic effect in realizing H$_2$ desorption of MgH$_2$ using solar irradiation as the only energy input (Figure 4d).

The solar-driven reversible H$_2$ storage performance of MgH$_2$, a key challenging aspect for the practical application, is subsequently investigated under the catalysis of Cu@MXene. Under the light density of 4.00 W cm^{-2}, the operating temperature for H$_2$ desorption and absorption of MgH$_2$ is determined to be approximately 275 and 240 °C, respectively (Figure S21, Supporting Information). Impressively, a reversible capacity of 5.9 wt% could be achieved for MgH$_2$ catalyzed with Cu@MXene after 30 cycles of H$_2$ adsorption and desorption, corresponding to a capacity retention of 91% (Figure 4e), and the reversible formation of MgH$_2$ after the first cycle of H$_2$ adsorption could be clearly demonstrated by XRD results (Figure S22, Supporting Information). More importantly, the H$_2$ desorption kinetics of MgH$_2$ under the catalysis of Cu@MXene is well-preserved after 30 cycles of hydrogen storage process (Figure S21c, Supporting Information), indicating its excellent stability of the photothermal and catalytic effect of Cu@MXene
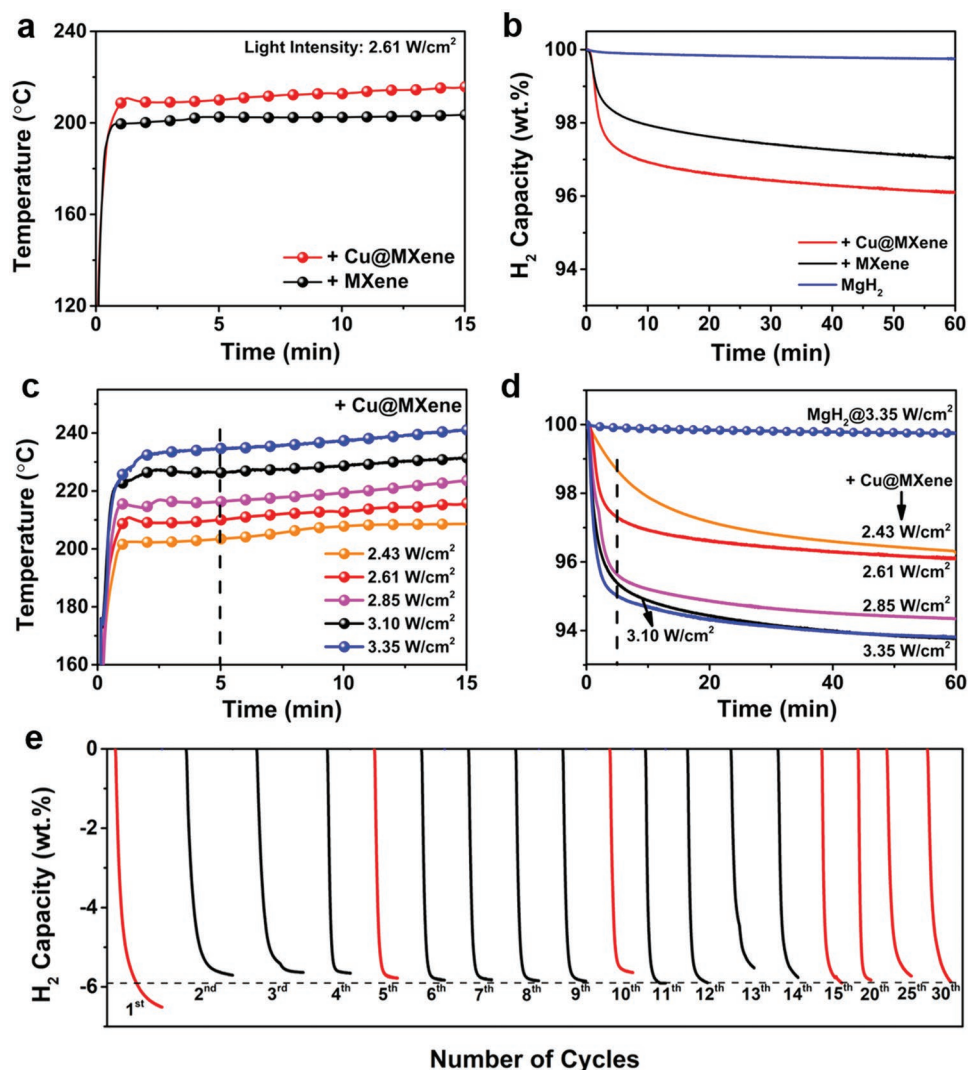
**ADVANCED
SCIENCE NEWS**

www.advancedsciencenews.com

**ADVANCED
MATERIALS**

www.advmat.de

Figure 4. a) The response of temperature to light irradiation and b) the corresponding H_2 desorption curves of MgH_2 under the catalysis of Cu@MXene and MXene, with pure MgH_2 included for comparison. c) The response of temperature to light irradiation and d) the corresponding H_2 desorption curves of MgH_2 under the catalysis of Cu@MXene under different light intensities. e) Cycling H_2 desorption curves of MgH_2 under the catalysis of Cu@MXene using a light intensity of 4 W cm^{-2}.

(**Figure 5**a). This result corresponds well with the stable cycling performance of MgH_2 under the catalysis of Cu@MXene upon thermal heating (Figure S10, Supporting Information), which indirectly demonstrates the excellent stability of the catalytic effect of Cu@MXene attributed to the space-confinement role of MXene nanosheets in inhibiting the agglomeration of catalytic Ti/TiH$_x$ species and photothermal Cu nanoparticles. On the other hand, nearly no change of the absorbance performance could be observed for MgH_2 under the catalysis of Cu@MXene after 15 cycles of H_2 adsorption process compared with its pristine ball-milled state (Figure S18d, Supporting Information), indicating the well-preserved photothermal effect, which is indispensable to drive reversible hydrogen storage reaction of MgH_2 using solar irradiation. In addition, it is interesting to note that the thermal conductivity of powdery MgH_2 is less than 1 W (m K)$^{-1}$,[30] which is far below that of Cu (397 W (m K)$^{-1}$) and MXene (55.8 W (m K)$^{-1}$).[31] Thus, under the catalysis

of Cu@MXene, MgH_2 with poor thermal conductivity could act as "heat isolator" to reduce the temperature gradient near Cu@MXene that acts as "nanoheater" and effective catalysts, which could contribute to driving fast H_2 desorption and absorption reactions of MgH_2.[32] As a result, MgH_2 under the catalysis of Cu@MXene could release 4.9 wt% of H_2 within a time period of only 10 min when using solar irradiation with an intensity of 2.85 W cm^{-2} as the energy input, while a saturation time as long as 30 min is required for that of MgH_2 when using external heating as the energy input (Figure S23, Supporting Information). This result demonstrates that, in comparison to the typical thermal-promoted solid-state H_2 storage reaction, the combination of photothermal conversion with catalytic effect allows the catalysts to collect a heating source to reduce the temperature gradient near catalytic center and get a higher reactivity at local sites, resulting in faster response of H_2 desorption to the solar irradiation than that of traditional thermal heating.

**ADVANCED
SCIENCE NEWS**

www.advancedsciencenews.com

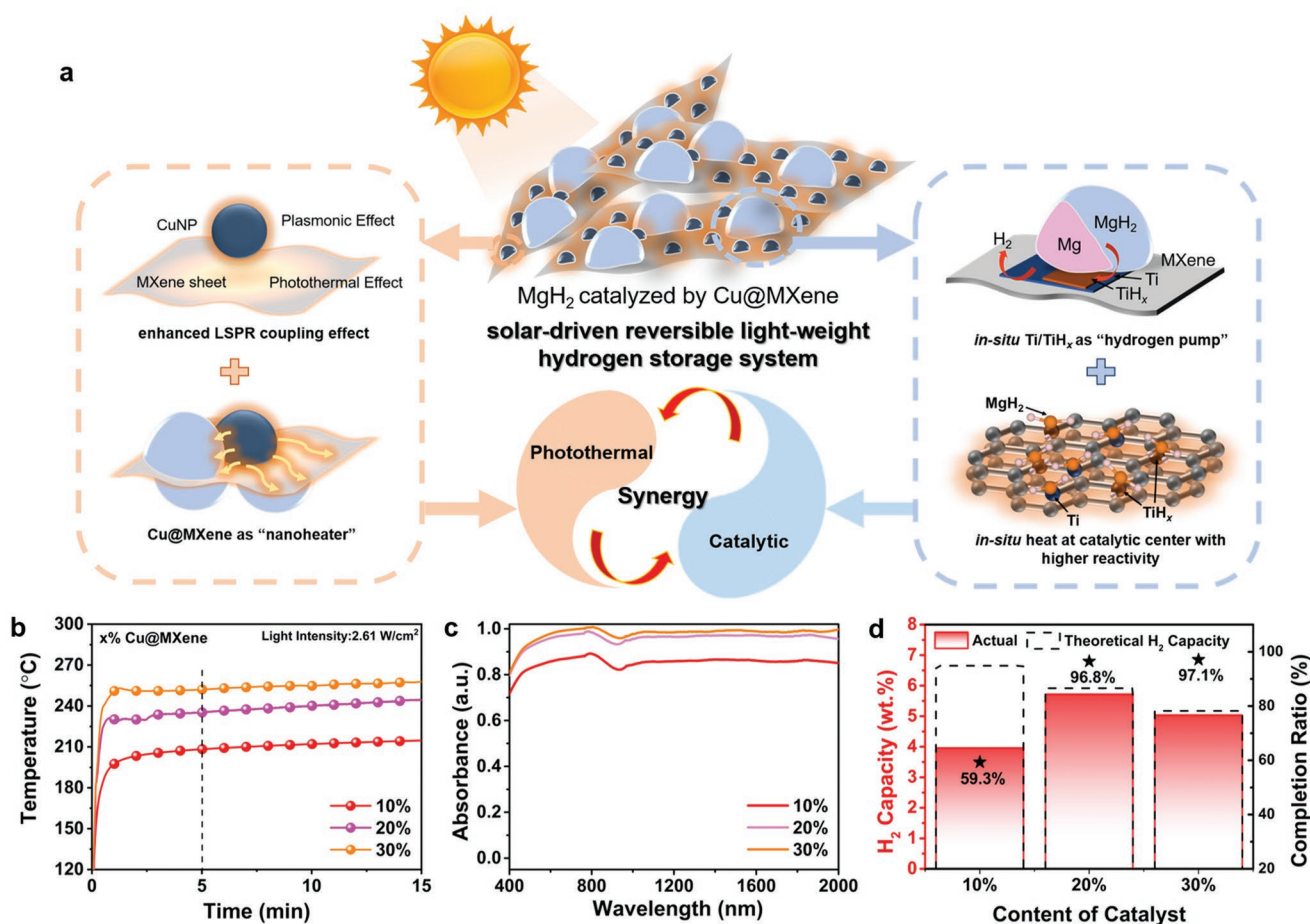**ADVANCED
MATERIALS**

www.advmat.de

Figure 5. a) Schematic diagram of the solar-driven reversible hydrogen storage of MgH$_2$ based on the photothermal and catalytic effect of Cu@MXene. b) The surface temperatures, c) UV–vis–NIR absorption spectra, and d) the comparison of H$_2$ desorption degree of MgH$_2$ under the catalysis of Cu@MXene with various ratios using a light intensity of 2.61 W cm^{-2}.

It is noted that the relatively high light intensity is required to drive the reversible hydrogen storage of MgH$_2$ even under the catalysis of Cu@MXene. Although high-intensity irradiation could be obtained by simply adding the Fresnel lens (j = 12 cm) to the Xenon lamp, for example, the low-intensity light (1.04–1.53 W cm^{-2}) could be concentrated to 3.73–5.70 W cm^{-2}, roughly increasing the light intensity to 3.6 times than that without any Fresnel lens, which makes it possible to drive reversible hydrogen storage reactions by natural light.[33] In order to verify this, an outdoor experiment of solar-driven H$_2$ desorption of MgH$_2$ under the catalysis of Cu@MXene using natural solar is performed via a low-cost PMMA Fresnel lens (j = 36) (Video S3 and Figure S24, Supporting Information). Hydrogen bubbles could be observed to dramatically emerge from the pipe upon the addition of the PMMA Fresnel lens, and more importantly, XRD results demonstrate that the main phase of MgH$_2$ catalyzed by Cu@MXene is Mg after this H$_2$ desorption process (Figure S24e, Supporting Information). These results provide direct evidence to the feasibility of driving solid-state hydrogen storage of MgH$_2$ by natural solar energy. However, the economy and the maximization of photothermal efficiency of this strategy should be further investigated in the future toward enhanced hydrogen storage performance of MgH$_2$ using natural solar as the only energy source. Taking Cu@MXene as an example, the effect of catalysts with various ratios is further explored for solar-driven H$_2$ storage of MgH$_2$. As expected, the increase of the loading ratio of Cu@MXene leads to the elevation of the stable temperature under the same illumination intensity (Figure 5b) due to the increase of its absorbance ability of the composite. As a result, upon increasing the loading ratio of Cu@MXene to 20%, the temperature of MgH$_2$ could be elevated to 235.6 °C, 27.3 °C higher than that with a loading ratio of Cu@MXene of 10%. The increase of temperature of MgH$_2$, however, is limited to 16.5 °C upon increasing the loading ratio of Cu@MXene to 30% from 20%, indicating the decreased efficiency of Cu@MXene in elevating the temperature of MgH$_2$ via increasing loading ratios. On the other hand, the increase of the loading ratio of Cu@MXene would decrease the systematic H$_2$ storage capacity down to 4.9 wt% (Figure S24, Supporting Information). Accordingly, the balance between photothermal effect of Cu@MXene and the systematic H$_2$ storage capacity should be optimized for practical applications. For instance, under a low light intensity of 2.61 W cm^{-2}, the hydrogen release amount of MgH$_2$ containing 20% of Cu@MXene reaches the best, with an H$_2$ desorption degree of 96.8%, which is close to saturation

(Figure 5d). By comparison, MgH_2 with a loading ratio of 10% of Cu@MXene could not reach the required temperature for its complete dehydrogenation owing to the limited photothermal effect. Although the increase of the loading ratio of Cu@MXene to 30% would result in a higher H_2 desorption degree of 97.1%, the theoretical H_2 capacity of this system would be significantly decreased to approximately 5.2 wt% H_2. More importantly, the increase of Cu@MXene could facile increase the normalized H_2 capacity released from sample pellets with higher thickness (Figures S26, S27, Supporting Information), and the differences of H_2 capacity released from sample pellets that exhibits adjacent thicknesses are much lower than that with a weight ratio of Cu@MXene of 10% (Table S4, Supporting Information). In particular, after doubling the thickness of the sample pellet from 0.16 to 0.31 mm, the normalized H_2 capacity loss for the sample pellet with a weight ratio of Cu@MXene of 10% reaches 18.3%, while this value could be reduced to 10.8% after increasing the weight ratio of Cu@MXene to 20%. Therefore, when designing a solar-driven hydrogen storage system, it is necessary to consider the balance between the photothermal conversion efficiency and the thus-obtained systematic hydrogen storage capacity.

3. Conclusions

This work creatively presents a strategy to realize solar-driven reversible hydrogen storage of light-weight metal hydrides based on the combination of the photothermal and catalytic effect. Specifically, Cu nanoparticles uniformly supported on MXene that combines plasmonic properties of Cu nanoparticles and the photothermal effect and high thermal conductivity of MXene nanosheets are constructed to realize solar-driven reversible hydrogen storage of MgH_2. The high photothermal conversion of Cu@MXene is able to generate localized heat under solar irradiation for thermally driving H_2 desorption and adsorption of MgH_2. On the other hand, the favorable interaction between MgH_2 and Cu@MXene results in the in situ formation of Ti and TiH_x species distributed on the surface of MXene, which are capable of effectively weakening Mg—H bonds, and meanwhile, the "hydrogen pump" effect of thus-formed Ti and TiH_x species significantly decreases the relative energy barrier of H_2 desorption from MgH_2. These synergistic effects lead to the significant decrease of the operating temperature required for dehydrogenation and hydrogenation of MgH_2. More importantly, due to its poor thermal conductivity, MgH_2 itself could act as "heat isolator" to reduce the temperature gradient near Cu@MXene that acts as the photothermal and catalytic sites, which contributes to driving fast H_2 desorption and absorption of MgH_2. Hence, the combination of high photothermal conversion with effective catalytic effect allows Cu@MXene to collect a heating source to reduce the temperature gradient near catalytic center and get a higher reactivity at local sites, leading to faster response of H_2 desorption to the solar irradiation than that of traditional thermal heating. Consequently, reversible hydrogen desorption and adsorption could be facile achieved for MgH_2 under the catalysis of Cu@MXene by using solar energy only. Our study on solar-driven hydrogen storage of metal hydrides may enlighten the interests

in developing new solid-state hydrogen storage technologies and solar-to-chemical energy reactions.

Supporting Information

Supporting Information is available from the Wiley Online Library or from the author.

Conflict of Interest

The authors declare no conflict of interest.

Data Availability Statement

The data that support the findings of this study are available in the supplementary material of this article.

[1] a) N. Abas, A. Kalair, N. Khan, *Futures* **2015**, *69*, 31; b) S. Chu, Y. Cui, N. Liu, *Nat. Mater.* **2017**, *16*, 16.

[2] a) I. Jain, *Int. J. Hydrogen Energy* **2009**, *34*, 7368; b) I. Staffell, D. Scamman, A. V. Abad, P. Balcombe, P. E. Dodds, P. Ekins, N. Shah, K. R. Ward, *Energy Environ. Sci.* **2019**, *12*, 463.

[3] a) U. Eberle, M. Felderhoff, F. Schueth, *Angew. Chem., Int. Ed.* **2009**, *48*, 6608; b) T. He, H. Cao, P. Chen, *Adv. Mater.* **2019**, *31*, 1902757.

[4] a) H. Wang, H. Lin, W. Cai, L. Ouyang, M. Zhu, *J. Alloys Compd.* **2016**, *658*, 280; b) Y. Sun, C. Shen, Q. Lai, W. Liu, D.-W. Wang, K.-F. Aguey-Zinsou, *Energy Storage Mater.* **2018**, *10*, 168; c) X. Yu, Z. Tang, D. Sun, L. Ouyang, M. Zhu, *Prog. Mater. Sci.* **2017**, *88*, 1.

[5] a) H. Reardon, J. M. Hanlon, R. W. Hughes, A. Godula-Jopek, T. K. Mandal, D. H. Gregory, *Energy Environ. Sci.* **2012**, *5*, 5951; b) Y. Jia, C. Sun, S. Shen, J. Zou, S. S. Mao, X. Yao, *Renewable Sustainable Energy Rev.* **2015**, *44*, 289.

[6] a) O. Morton, *Nature* **2006**, *443*, 19; b) N. Kannan, D. Vakeesan, *Renewable Sustainable Energy Rev.* **2016**, *62*, 1092.

[7] a) M. Chen, Y. He, J. Huang, J. Zhu, *Energy Convers. Manage.* **2016**, *127*, 293; b) Y. Gutiérrez, M. Losurdo, F. González, H. O. Everitt, F. Moreno, *J. Phys. Chem. C* **2020**, *124*, 7386.

[8] a) H. Zhang, H. Xia, Y. Zhao, *J. Mater. Chem.* **2012**, *22*, 845; b) X. Chong, N. Jiang, Z. Zhang, S. Roy, J. R. Gord, *J. Nanopart. Res.* **2013**, *15*, 1678.

[9] a) J. Ran, G. Gao, F.-T. Li, T.-Y. Ma, A. Du, S.-Z. Qiao, *Nat. Commun.* **2017**, *8*, 13907; b) L. Yao, Q. Gu, X. Yu, *ACS Nano* **2021**, *15*, 3228.

[10] a) M. Xu, S. Lei, J. Qi, Q. Dou, L. Liu, Y. Lu, Q. Huang, S. Shi, X. Yan, *ACS Nano* **2018**, *12*, 3733; b) H. Li, X. Li, J. Liang, Y. Chen, *Adv. Energy Mater.* **2019**, *9*, 1803987.

[11] M. Liu, W. Zhou, T. Wang, D. Wang, L. Liu, J. Ye, *Chem. Commun.* **2016**, *52*, 4694.

[12] a) H. Miao, D. Zhong, Z. Zhou, X. Yang, *Nanoscale* **2015**, *7*, 19066; b) T. López, J. L. Cuevas, L. Ilharco, P. Ramírez, F. Rodríguez-Reinoso, E. Rodríguez-Castellón, *Mol. Catal.* **2018**, *449*, 62.

[13] a) J.-C. Lei, X. Zhang, Z. Zhou, *Front. Phys.* **2015**, *10*, 276; b) D. Wang, F. Li, R. Lian, J. Xu, D. Kan, Y. Liu, G. Chen, Y. Gogotsi, Y. Wei, *ACS Nano* **2019**, *13*, 11078.

[14] a) S. Kim, J. M. Kim, J. E. Park, J. M. Nam, *Adv. Mater.* **2018**, *30*, 1704528; b) Y. Xin, K. Yu, L. Zhang, Y. Yang, H. Yuan, H. Li, L. Wang, J. Zeng, *Adv. Mater.* **2021**, *33*, 2008145.

[15] a) Z. Zhu, Y. Zou, W. Hu, Y. Li, Y. Gu, B. Cao, N. Guo, L. Wang, J. Song, S. Zhang, *Adv. Funct. Mater.* **2016**, *26*, 1793; b) X. Fan, L. Liu, X. Jin, W. Wang, S. Zhang, B. Tang, *J. Mater. Chem. A* **2019**, *7*, 14319.

[16] a) C. Wang, Y. Wang, X. Jiang, J. Xu, W. Huang, F. Zhang, J. Liu, F. Yang, Y. Song, Y. Ge, *Adv. Opt. Mater.* **2019**, *7*, 1900060; b) D. Xu, Z. Li, L. Li, J. Wang, *Adv. Funct. Mater.* **2020**, *30*, 2000712.

[17] R. Li, L. Zhang, L. Shi, P. Wang, *ACS Nano* **2017**, *11*, 3752.

[18] a) C. Liu, H. Zhang, R. Li, X. Li, G. Yang, *Chem. Eng. J.* **2020**, *420*, 127672; b) Z. Yu, L. Jiang, R. Liu, W. Zhao, Z. Yang, J. Zhang, S. Jin, *Chem. Eng. J.* **2021**, *426*, 131914.

[19] a) X. Guo, C. Hao, G. Jin, H. Y. Zhu, X. Y. Guo, *Angew. Chem., Int. Ed.* **2014**, *53*, 1973; b) C. Crane, F. Wang, J. Li, J. Tao, Y. Zhu, J. Chen, *J. Phys. Chem. C* **2017**, *121*, 5684; c) S. Zhao, Z. Cheng, S. Wang, H. Hao, Y. Fang, *Appl. Phys. A* **2021**, *127*, 930.

[20] Z. Wu, C. Li, Z. Li, K. Feng, M. Cai, D. Zhang, S. Wang, M. Chu, C. Zhang, J. Shen, Z. Huang, Y. Xiao, G. A. Ozin, X. Zhang, L. He, *ACS Nano* **2021**, *15*, 5696.

[21] a) A. W. Hauser, A. A. Evans, J. H. Na, R. C. Hayward, *Angew. Chem., Int. Ed.* **2015**, *127*, 5524; b) T. Zhang, Y. Che, K. Chen, J. Xu, Y. Xu, T. Wen, G. Lu, X. Liu, B. Wang, X. Xu, *Nat. Commun.* **2020**, *11*, 3027.

[22] X. Fan, Y. Ding, Y. Liu, J. Liang, Y. Chen, *ACS Nano* **2019**, *13*, 8124.

[23] a) X. Zhang, Y. Liu, X. Zhang, J. Hu, M. Gao, H. Pan, *Mater. Today Nano* **2020**, *9*, 100064; b) T. Sadhasivam, H.-T. Kim, S. Jung, S.-H. Roh, J.-H. Park, H.-Y. Jung, *Renewable Sustainable Energy Rev.* **2017**, *72*, 523.

[24] a) B. Peng, J. Liang, Z. Tao, J. Chen, *J. Mater. Chem.* **2009**, *19*, 2877; b) F. Cheng, Z. Tao, J. Liang, J. Chen, *Chem. Commun.* **2012**, *48*, 7334.

[25] V. Berezovets, R. Denys, I. Y. Zavaliy, Y. V. Kosarchyn, *Int. J. Hydrogen Energy* **2022**, *47*, 7289.

[26] a) D. Großmann, K. Klementiev, I. Sinev, W. Grünert, *ChemCatChem* **2017**, *9*, 365; b) H. Liu, C. Lu, X. Wang, L. Xu, X. Huang, X. Wang, H. Ning, Z. Lan, J. Guo, *ACS Appl. Mater. Interfaces* **2021**, *13*, 13235.

[27] a) Y. Liu, H. Du, X. Zhang, Y. Yang, M. Gao, H. Pan, *Chem. Commun.* **2016**, *52*, 705; b) W. Zhu, L. Ren, C. Lu, H. Xu, F. Sun, Z. Ma, J. Zou, *ACS Nano* **2021**, *15*, 18494.

[28] D. Mateo, J. L. Cerrillo, S. Durini, J. Gascon, *Chem. Soc. Rev.* **2021**, *50*, 2173.

[29] G. Chen, R. Gao, Y. Zhao, Z. Li, G. I. Waterhouse, R. Shi, J. Zhao, M. Zhang, L. Shang, G. Sheng, *Adv. Mater.* **2018**, *30*, 1704663.

[30] G. Xia, Y. Tan, X. Chen, D. Sun, Z. Guo, H. Liu, L. Ouyang, M. Zhu, X. Yu, *Adv. Mater.* **2015**, *27*, 5981.

[31] Z. Li, H. Zhang, J. Han, Y. Chen, H. Lin, T. Yang, *Adv. Mater.* **2018**, *30*, 1870185.

[32] Y. Chen, Y. Zhang, G. Fan, L. Song, G. Jia, H. Huang, S. Ouyang, J. Ye, Z. Li, Z. Zou, *Joule* **2021**, *5*, 3235.

[33] a) P. Gleckman, J. O'Gallagher, R. Winston, *Nature* **1989**, *339*, 198; b) R. J. Braham, A. T. Harris, *Ind. Eng. Chem. Res.* **2009**, *48*, 8890.